2017 MERIT Self-directed Joint Research

Elucidation and Control of Defects in $(ZnSe)_{0.85}(CuIn_{0.7}Ga_{0.3}Se_2)_{0.15}$ Photocathode for Solar Hydrogen Production

Dept. of Chemical System Engineering, D3, Ayako Kubo
Dept. of Chemical System Engineering, D2, Hiroyuki Kaneko

Abstract

In this study, we aimed to investigate the structures and properties of point defects in the novel p-type photocathode semiconductor thin film, $(ZnSe)_{0.85}(CuIn_{0.7}Ga_{0.3}Se_2)_{0.15}$, which is used for the water splitting under visible light irradiation, by means of first principle calculation. As a result, we identified the defect structure from which the p-type characteristics of this material originates. We also showed that its p-type characteristics will be improved under Cu-rich conditions. Furthermore, from a thermodynamic consideration, we clarified the relationship between the crystal growth of ZnSe/CIGS and the growth conditions such as temperatures and partial pressures. All these results support the relevant experimental results, and will give guidelines to control the properties of ZnSe/CIGS in the future.

Authors

Ayako Kubo: She belongs to Yamashita-Ushiyama laboratory. She is specialized in first principle calculations and is working on theoretical investigations on photocatalysts that consist of oxynitrides and solid-solutions. In this work, she mainly contributed to the calculations on the defect structural models of the photocathode solid solution $(ZnSe)_{0.85}(CuIn_{0.7}Ga_{0.3}Se_2)_{0.15}$.

Hiroyuki Kaneko: He belongs to Domen-Minegishi laboratory, is specialized in semiconductor electrodes and is working on construction of efficient and durable photoelectrochemical system. In this work, he mainly contributed to preparation condition of solid solution thin films.

1. Introduction

Recently, hydrogen productions from water splitting in photoelectrode system is getting wide attention [1], since their abilities to convert the solar energies into hydrogen fuels, which are storable and transportable energy carriers, only using a simple system. In the previous study, Kaneko *et al.* developed $(ZnSe)_{0.85}(CuIn_{0.7}Ga_{0.3}Se_2)_{0.15}$ (hereafter ZnSe/CIGS) thin films as a photocathode material used for hydrogen evolution in the photoelectrode system [2][3]. ZnSe/CIGS is a p-type semiconductor material, and was synthesized by co-evaporation method onto a soda-lime glass substrate. ZnSe/CIGS can be regarded as a solid solution between CIGS, a

conventional photocathode material with a chalcopyrite structure, and zinc blende type ZnSe, whose basic structure is in common with that of chalcopyrites. Kaneko *et al.* have shown that ZnSe/CIGS achieves band edge positions which is suitable for water splitting with relatively high onset potential 0.9 V_{RHE} when ZnSe/(ZnSe+CIGS) ratio is 0.85.

In general, photocathodes materials consist of p-type semiconductors, and their p-type characteristics originate from point defects in their crystals. However, the behaviors of the point defects in ZnSe/CIGS have not been well studied yet, and thus the origin of its p-type characteristics is unraveled. For example, the origin of the p-type characteristics of the conventional photocathode CIGS are known to be Cu vacancy (V_{Cu}) acceptors in the CIGS crystal [4]. However, since the atomic content of Cu in ZnSe/CIGS crystal is only up to 15 %, and some antisite defects such as Zn_{Cu} can also be created, V_{Cu} is unlikely a dominant origin of the p-type characteristics of this material. Furthermore, while CIGS shows improved p-type characteristics under Cu-poor conditions, ZnSe/CIGS shows n-type characteristics under the same condition [5]. These differences can be caused by the difference in the dominant defects in their crystals, solid solution (ZnSe/CIGS) and non-solid solution (CIGS), but this has not been confirmed by experiments.

Here, in this research, we aimed to clarify the structures and properties of point defects in ZnSe/CIGS solid solution by means of first principle calculations. In particular, we will identify the dominant defect that determines the properties of ZnSe/CIGS by evaluating and comparing the formation energies of various defect structures. Furthermore, we will estimate the concentrations of each defect and carriers from the calculated formation energies, to predict their dependency on growth conditions such as temperature and partial pressures, and thus compare them to experimental results.

2. Methods

2.1. First principle calculations

In our study, we prepared a structural model of ZnSe/CIGS solid solution, and compared the defect formation energies by using first principle calculations. Then, we investigated the dependency of the defect formation energies on the temperature and partial pressures to compare the results between calculations and experiments.

First, we prepared the structural model of the bulk ZnSe/CIGS solid solution as shown in figure.1. The structure is created by multiplying the unit cell of ZnSe (cubic, a =3.9739 Å, 8

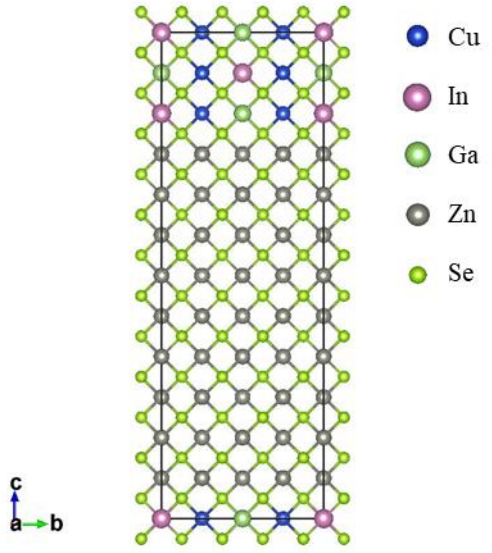

Figure 1. The structural model of ZnSe/CIGS

atoms [6]) to make 2 × 2 × 6 supercell (192 atoms), and substituted one fourth of its Zn atoms by Cu, In, and Ga atoms. Here, Zn/Cu ratio was fixed to 6/1 to reflect the experimental value (15 %). The cationic arrangements of Cu, In, Ga were determined in accordance with octet rule, which was also followed in the previous study on CIGS first principle calculations [7]. Thus, we prepared several structural models of bulk ZnSe/CIGS with different cationic arrangements, and adopted the most stable one. Here, we confirmed that the structures which do not follow the octet rule are unstable compared to those which follow the rule by 100 meV per formula unit by the calculations.

Subsequently, by using the ZnSe/CIGS bulk model above, we prepared several defect structural models. We considered four types of vacancies (V_{Zn}, V_{Cu}, V_{In}, V_{Ga}), ten types of antisites (Cu_{Zn}, In_{Zn}, Ga_{Zn}, Zn_{Cu}, In_{Cu}, Ga_{Cu}, Zn_{In}, Cu_{In}, Zn_{Ga}, Cu_{Ga}), and one interstitial Se_{int} as defect models in ZnSe/CIGS. Here, the concentration of the defects was set to 1 %.

By using the defect structural models prepared as described above, we calculated the defect formation energy that is defined by the following equation.

$$(1)\quad E_f(D^q) = E(D^q) - E_p - \sum n_i\mu_i + q(\varepsilon_{VBM} + \varepsilon_F)$$

$E(D^q)$ is a total energy of the defect structural model with charge q, E_p is a total energy of the bulk structural model, n_i is the number of reduced or added atoms of element i, μ_i is the chemical potential of element i, and ε_F is the Fermi energy which is referenced to VBM(Valence Band Maximum). As defect charges, we considered the positive ones for donor defect models (which depicts the situations that the defect had donated the

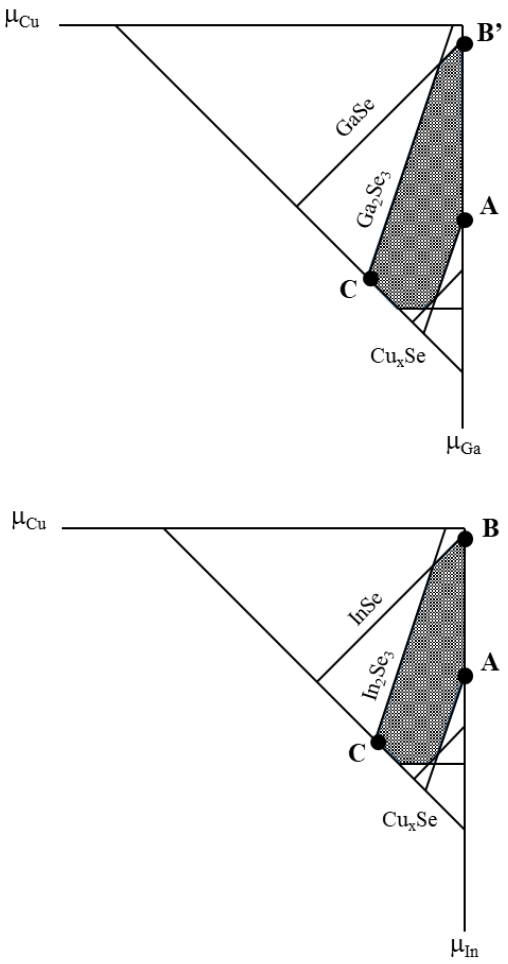

Figure 2. The value ranges of each chemical potential.

Table 1. Partial pressures and chemical potentials of each element calculated from the experimental conditions (450 ℃)

i	Cu	In	Ga	Zn	Se
p_i ($\times 10^{-4}$ Pa)	1	1.3	0.4	4	7
μ_i (eV)	1.1	0.1	0.3	-0.9	0.0

electrons) and negative ones for acceptor defect models (which depicts the situations that the defect had accepted the electrons). The value μ_i was referenced to the total energies of each elemental substance, and was determined by using a kind of phase diagram as explained in the following paragraph. The last term ε_F was regarded as a variable.

Chemical potentials were determined by using the phase diagram shown in figure 2. This diagram was depicted using the formation energies of the compounds that can be obtained as by-products in synthesizing ZnSe/CIGS. The region in the diagram that is marked with diagonal lines shows the value range of μ_{Zn}, μ_{Cu}, μ_{Ga}, μ_{In}, and μ_{Se}. Here, points A, B(B'), and C correspond to the Cu-rich condition, In-rich (Ga-rich) condition, and Se-rich condition, respectively.

On the other hand, chemical potentials can be estimated from the experimental conditions by using the following equation.

$$(2)\ \ \mu_i(\mathrm{T}) = \mu_i^o(T) + RTln\frac{p_i}{p^o}$$

$$(3)\ \ \mu_i^o(T) = \Delta_f G_i^o - TS^o$$

$\Delta_f G^o_i$ is a standard molar Gibbs energy of element i (literature data [8]), p^o is a total pressure under a standard condition (= 1 atm), p_i is the partial pressure of element i, and T is a temperature. Using these formulas, we estimated the chemical potential of each element in the vapor deposition beams under the synthesize condition of this material. The partial pressures of each element are estimated from their deposition rates. The partial pressures and chemical potentials are listed in table 1. Here, since μ_{Cu} is the largest (+1.1 eV) and μ_{Zn} is the smallest (-0.9 eV), the chemical potentials of each elements in this material correspond to point A in figure 2. Therefore, we use the chemical potentials at the point A ((μ_{Cu}, μ_{In}, μ_{Ga}, μ_{Zn}, μ_{Se}) = (0.0, -1.1, -1.4, -1.0, -0.6)) in the following section to calculate the defect formation energies.

All the calculations were done by means of the density functional theory (DFT) with the projector augmented wave (PAW) method and the localized density approximation (LDA) exchange-correlation functional. For Cu, In, Ga, and Zn, s and p electrons in the outermost shell and d electrons just below these electrons were treated as valence states. For Se, 4s and 4p electrons were treated as valence states. *k*-point sampling was set to 2 × 2 × 1 and the 400 eV cutoff energy were used. Besides, in order to describe the d-electrons nearby the defects more precisely, we added onsite Coulomb potential to Zn (U = 7.0 eV), Cu (U = 6.0 eV), In (U = 7.0 eV) and Ga (U = 9.0 eV), so that the positions of their d-band peak in the valence bands will reproduce the experimental data [9][10]

2.2. Preparation of ZnSe/CIGS thin films

The soda-lime glass coated with a 500 nm-thick Mo was used as a substrate, which was prepared by RF magnetron sputtering of Mo onto the soda-lime glass. Elemental Cu (0.032~0.045 nm s^{-1}), In (0.048 nm s^{-1}), Ga (0.014 nm s^{-1}), Zn (0.3~0.4 nm s^{-1}) and Se (1 nm s^{-1}) were deposited onto the substrate,

resulting in formation of ZnSe/CIGS thin films in a high vacuum chamber.[2] It should be noted that we employed excess amount of Cu, Zn and Se because Zn and Se show relatively high vapor pressure and it has been reported that excess amount of Cu causes formation of p-type ZnSe/CIGS. Subsequently, the samples were dipped into an etching solution containing KCN to remove Cu_xSe on the film surface.

The ZnSe/CIGS thin films were analyzed using a scanning electron microscope (S-4700, Hitachi).

3. Results and Discussion

First, formation energies of each defect are plotted in figure 3. The formation energies of six antisites, Cu_{Zn}, In_{Zn}, Ga_{Zn}, Zn_{Cu}, Zn_{In}, Zn_{Ga} are especially small (Figure 3b). None of these antisites can be created in ZnSe nor CIGS itself, but can only be created in the solid solution. Besides, since the formation energies of these antisites are much smaller than that of V_{Cu} (figure 3a), a well-known acceptor that gives p-type characteristics to CIGS, they are presumed to be the dominant defects in ZnSe/CIGS crystal which can be easily created.

Among these defects, In_{Zn}, Ga_{Zn}, and Zn_{Cu} work as donors, while Cu_{Zn}, Zn_{In}, and Zn_{Ga} work as acceptors. In figure 3b, the straight lines that correspond to the formation energies of these defects intersect at the energy position 0.4 eV above VBM (pointed with an arrow). This means that the position of its Fermi energy will be pinned nearby the intersection, since more donor will be created in the energy region of $\varepsilon_F < 0.4$ eV and more acceptors will be created in the energy region of $\varepsilon_F > 0.4$ eV, both of which cancel the variation of the Fermi energy. In this material, the position of the intersection is closer to VBM than CBM, and thus ZnSe/CIGS is thought to be a p-type semiconductor. This result supports the experimental fact that ZnSe/CIGS

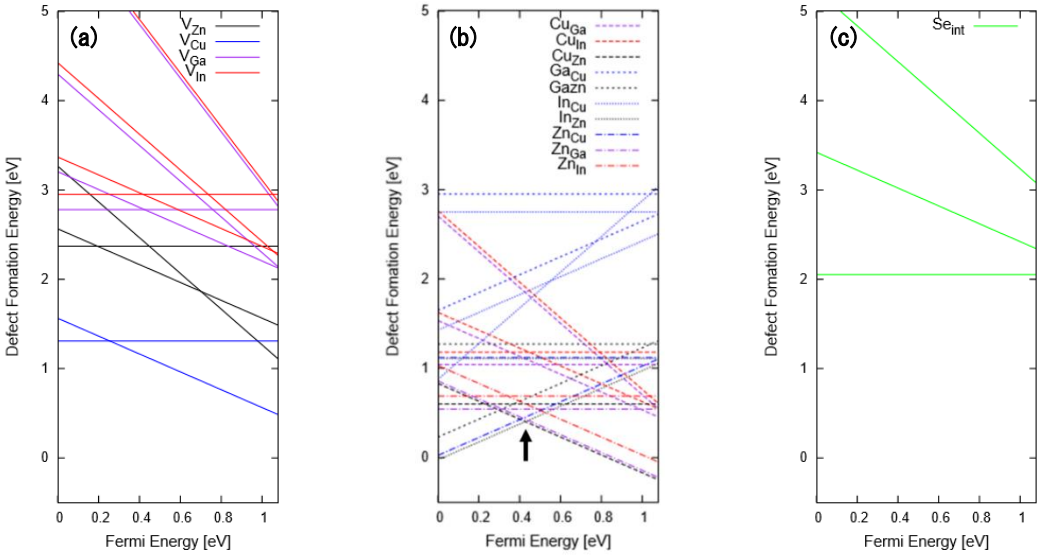

Figure 3. Formation energies of each defects. (a) Vacancies. (b) Antisites. (c) An interstitial. Chemical potential corresponds to point A in figure 2 was adopted.

Table 2. Chemical potentials of each element at each temperature.

	μ_{Cu}	μ_{In}	μ_{Ga}	μ_{Zn}	μ_{Se}
350℃	1.4	0.5	0.7	-0.6	0.3
450℃	1.1	0.1	0.3	-0.9	0.0
550℃	0.7	-0.2	0.0	-1.3	-0.4
650℃	0.4	-0.6	-0.4	-1.6	-0.7

has a p-type characteristic though ZnSe itself, which dominates more than 80% of this material, is essentially an n-type semiconductor.

Next, we will discuss the temperature dependency of the defect formation energy. Since in equation (1) only the term μ will be varied with temperature, here, we investigated the temperature dependency of the chemical potentials. The calculated chemical potentials of the vapor deposition beam at each temperature (350~650 ℃) are listed in table 2. For all the chemical elements, their chemical potentials decrease by 0.3 ~ 0.4 eV with increasing temperature by 100 ℃.

When the temperature rises above a certain level, the chemical potentials of the vapor deposition beams can become too low to shape a crystal. For example, above 550 ℃, the sum of μ_{Zn} and μ_{Se} is lower than the formation enthalpy of ZnSe (-1.62 eV), indicating that ZnSe crystal cannot be created thermodynamically among this temperature region.

Some experimental results also support that the crystallinity of ZnSe decreases by increasing temperature. For example, the SEM pictures in figure 4 show that the crystals of ZnSe/CIGS become rounded off above 550 ℃. In another experiment, it was observed that the photocurrent of ZnSe/CIGS was decreased with the increasing temperature above 550 ℃.

On the other hand, the sum of chemical potentials of μ_{Cu}, μ_{In}, μ_{Ga}, and μ_{Se} is always larger than the formation enthalpy of CIGS (-4.47 eV) among all temperature region. This means that CIGS can be crystalized under the high-temperature region above 550 ℃. Besides, since μ_{Cu} decreases with the increasing temperature, the formation energy of V_{Cu}, the most dominant defect in CIGS crystal, will also be decreased under the high-temperature condition according to equation (1). Therefore, the p-type characteristics of CIGS will be increased with the temperature. These results

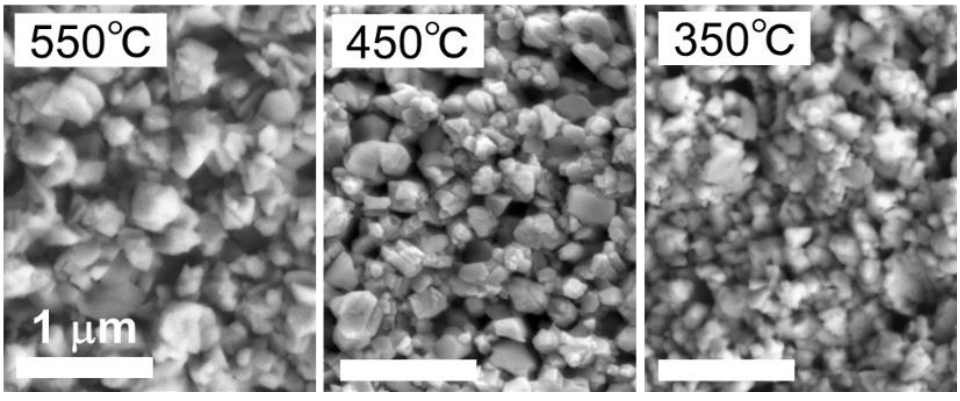

Figure 4. SEM images of ZnSe/CIGS thin films with different deposition temperature

agree with the experimental facts that CIGS itself shows greater photocurrent and photovoltaic power among higher temperature above 500 ℃, while the photocurrent of ZnSe/CIGS peaks out at 450 ℃.

Subsequently, we will discuss the dependency of the defect properties on partial pressures. Since the variations of the partial pressures will also be reflected in the chemical potentials, as shown in equation (2), we will only discuss the effects of the change in chemical potentials of certain elements on the defect formation energies. Besides, here, we will only consider the effect of the variation in Cu and Zn, which are the dominant cations in the solid solution. We will also investigate the carrier concentration under each condition.

First, we showed the defect formation energies with different μ_{Cu} in figure 5. For simplicity, we only plotted the formation energies of six dominant defects (Cu_{Zn}, In_{Zn}, Ga_{Zn}, Zn_{Cu}, Zn_{In}, Zn_{Ga}) mentioned above. As μ_{Cu} increases (= as p_{Cu} increases) the intersection between the straight lines that correspond to the formation energies of donors and acceptors get much closer to VBM. This is probably because the Cu_{Zn}, one of the dominant acceptors, becomes more easily to be created with increasing μ_{Cu}, while Cu_{Zn}, one of the dominant donors, gets less easily to be created in the same situation. On the other hand, the formation energies of the other dominant acceptors (Zn_{Ga}, Zn_{In}) and donors (In_{Zn}, Ga_{Zn}) remain unchanged. This result indicates that the p-type characteristics of ZnSe/CIGS will be increased with increasing p_{Cu}.

Hence, we subsequently estimated the variations of Fermi energy ε_F and the carrier concentration C_p in ZnSe/CIGS with increasing μ_{Cu}. Fermi energy ε_F and the carrier concentration C_p were calculated using following equations.

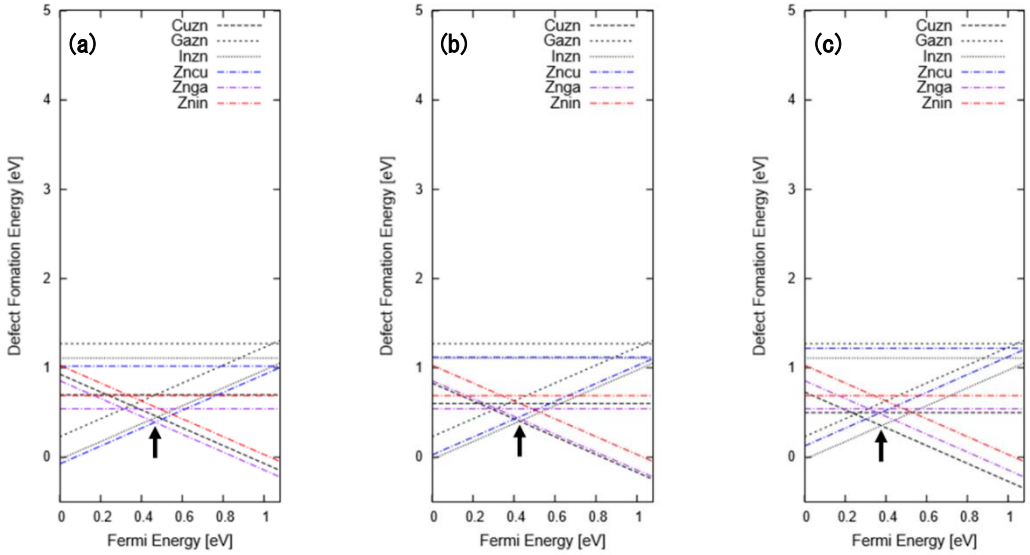

Figure 5. Comparison of defect formation energies with various μ_{Cu}.
(a) μ_{Cu} = −0.1 (b) μ_{Cu} = 0.0 (The same condition as figure 3) (c) μ_{Cu} = +0.1。

Table 3. Fermi energy and carrier concentration at each chemical potential μ_{Cu}.

μ_{Cu}	-0.1	0.0	+0.1
ε_F (eV)	0.46	0.42	0.38
C_p (cm^{-3})	1.49×10^{15}	2.75×10^{16}	5.61×10^{16}

Table 4. Fermi energy and carrier concentration at each chemical potential μ_{Zn}.

μ_{Zu}	-1.1	-1.0	-0.9
ε_F (eV)	0.43	0.42	0.40
C_p (cm^{-3})	2.34×10^{16}	2.75×10^{16}	4.15×10^{16}

(4) $\sum_{X,q}[D^q] - n + p = 0$

(Electrically neutral conditions)

(5) $C_p = -n + p$

(6) $[D^q] = N_0 \exp\left(-\frac{E_f(D^q)}{k_B T}\right)$

(7) $n = \left(-\frac{m_e^* k_B T}{2\pi\hbar^2}\right)^{\frac{3}{2}} \exp\left(-\frac{\varepsilon_{CBM} - \varepsilon_F}{k_B T}\right)$

(8) $p = \left(-\frac{m_h^* k_B T}{2\pi\hbar^2}\right)^{\frac{3}{2}} \exp\left(-\frac{\varepsilon_F}{k_B T}\right)$

$[D^q]$, n, and p are the concentrations of charged defect D^q, electron, and hole, respectively. Each of them is related to Fermi energy ε_F by following formulas.

The calculated ε_F and C_p was listed in table 3. As μ_{Cu} increases, ε_F gets lower and C_p gets larger. This result also strongly supports that the p-type characteristics of ZnSe/CIGS will be improved with increasing p_{Cu}.

Next, we showed the defect formation energies with different μ_{Zn} in figure 6. In contrast to the case for μ_{Cu}, the intersection between the lines of donors' and acceptors' formation energies is nearly unchanged with increasing μ_{Zn} (= increasing p_{Zn}). This is probably because the changes in the formation energies of the dominant donors (In_{Zn}, Ga_{Zn}, Zn_{Cu}) and the dominant acceptors (Cu_{Zn}, Zn_{In},

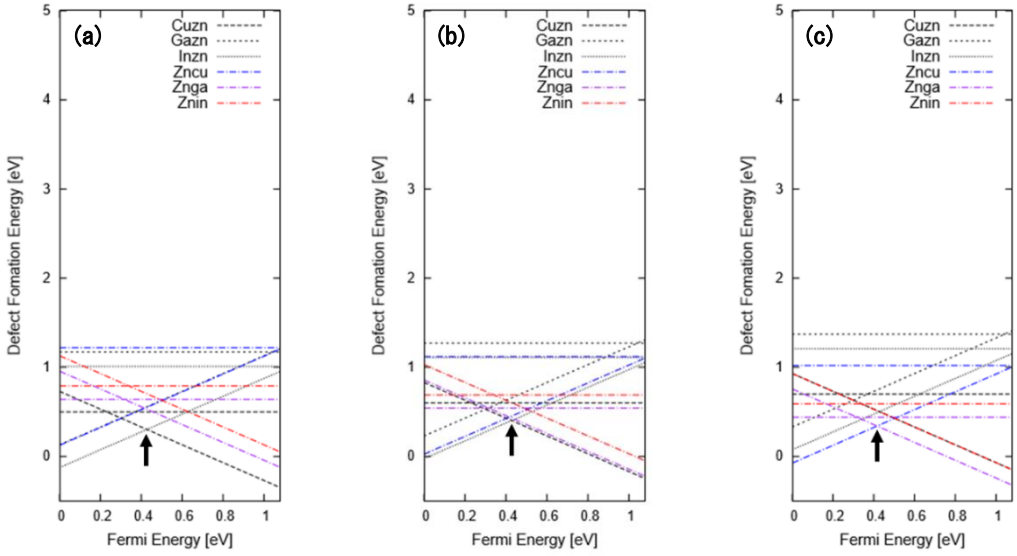

Figure 6. Comparison of defect formation energies with various μ_{Zn}.

(a) μ_{Zn} = -1.1 (b) μ_{Zn} = -1.0 (The same condition as figure 3) (c) μ_{Zn} = -0.9。

Zn_{Ga}) with increasing μ_{Zn} were cancelled. Therefore, it is expected that the p-type characteristics of ZnSe/CIGS will hardly change with increasing p_{Zn}. The variations of ε_F and C_p with increasing μ_{Zn} also show the same trend (table 4).

Experimentally, as mentioned in the opening sentences, some results show that ZnSe/CIGS acheives n-type characteristics under Cu-poor conditions. This trend aligns with the results of the first principle calculation above [4]. Furthermore, the photocurrent was observed to be improved with increasing Cu supply ($J_{Cu}/J_{In}+J_{Ga}$) to a certain degree [5] (figure 7). It should be noted that, as explained in detail in the following section, in this case the cationic ratio Zn/Ga+In was also increased with increasing $J_{Cu}/J_{In}+J_{Ga}$ (figure 8). However, since the effect of the change in μ_{Zn} on the p-type characteristics of this material is expected to be small, the improved photocurrent can be attributed to the suppression of Zn_{Cu} donors and promotion of Cu_{Zn} acceptors with increasing μ_{Cu}.

Last of all, we will discuss the interplay between the chemical potentials μ_{Cu} and μ_{Zn}. As mentioned above, when Cu supply ($J_{Cu}/J_{In}+J_{Ga}$) was increased, the cationic ratio Zn/Ga+In was also increased, although the cationic ratio Cu/Ga+In remained almost unchanged. In figure 8, we plotted the ratio Zn/Ga+In at each Cu supply. Although the supply of Zn was fixed as constant, the relative amount of Zn proportionally increased with Cu supply. Besides, the ratio did not change after the post-processing using KCN aqueous solution to remove Cu_xSe. Therefore, it was confirmed that

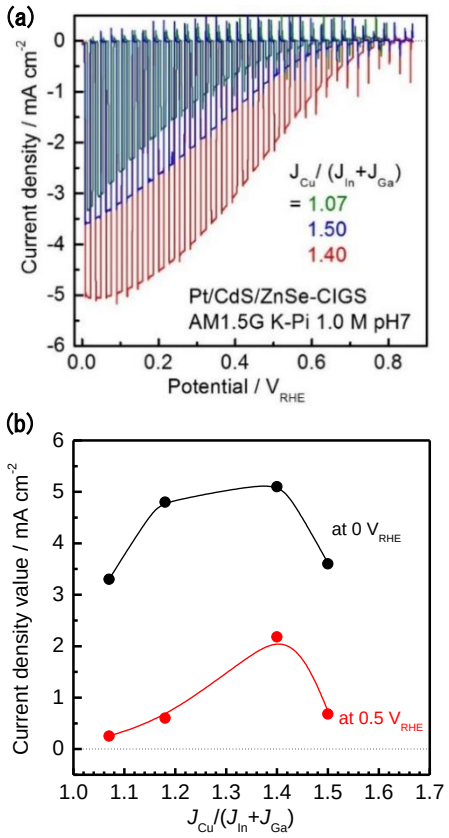

Figure 7. (a) I-V curves with $J_{Cu}/J_{In}+J_{Ga}$ = 1.07, 1.4 and 1.50 (b) Photocurrent densities at each $J_{Cu}/J_{In}+J_{Ga}$ ratio.

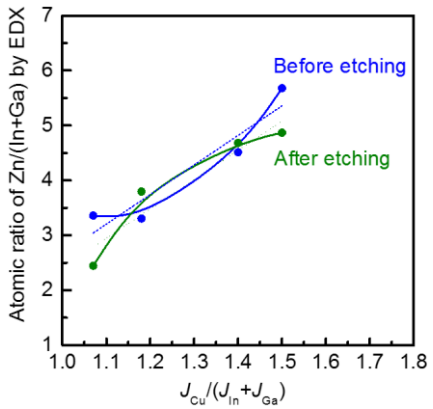

Figure 8. Relationship between atomic ratio of Cu/(In+Ga) in the molecular beam (x-axis) and atomic ratio of Zn/(In+Ga) in ZnSe/CIGS thin films observed by EDX analysis before (blue) and after (green) KCN etching process.

the increase of Zn/Ga+In ratio occurred in ZnSe/CIGS thin film itself. We will discuss on this trend from thermodynamic point of view in the next paragraph.

First, the ratio of Cu/Ga+In was fixed due to the octet rule. When Cu/Ga+In deviates from one, it breaks the octet rule and the structure will be thermodynamically unstable. Redundant Cu was experimentally observed to segregate as Cu_xSe at the surface of the material.

Next, we focus on the change in each chemical potential when the supply of Cu was increased. Under the condition where CIGS can thermodynamically be crystalized, μ_{Se} decreases as μ_{Cu} increases. On the other hand, since under the condition where ZnSe can be crystalized the sum of μ_{Se} and μ_{Zn} must remain constant, μ_{Zn} increases as μ_{Se} decreases. Therefore, among these conditions, μ_{Zn} will also be increased when μ_{Cu} was increased, and this is presumed to be the origin of the proportional increase of Zn amount with Cu supply. This indicates that we can indirectly control the introduction amount of Zn, an element with inherently high vapor pressure, by changing μ_{Cu}, which can be also applied in various types of solid solutions.

4. Concluding remarks

In this research, we investigated the dominant defect structures in p-type semiconductor ZnSe/CIGS, the solid solution of II-VI and I-III-VI_2 compound, by means of first principle calculations. As a result, we identified that the dominant defects in this material are the six antisites (Cu_{Zn}, In_{Zn}, Ga_{Zn}, Zn_{Cu}, Zn_{Ga}, Zn_{In}), and that three of them (Cu_{Zn}, Zn_{Ga}, Zn_{In}) are the acceptors that are the origins of the p-type characteristics of this material. Furthermore, we investigated the relationship between the formation energies of these defects and chemical potentials of Cu and Zn, and clarified that p-type characteristics will be improved in Cu-rich condition. The same trend was also observed in some experimental results.

Besides, from a thermodynamic consideration, we showed that ZnSe/CIGS can be stably crystalized under the temperature relatively lower than the synthetical condition of pure CIGS. We also demonstrated by considering the interplay between the chemical conditions of each elements that we can indirectly control the introduction amount of Zn into the solid solution only by changing the partial pressure of Cu.

Through this research, by clarifying the structures and properties of dominant defects and thermodynamic characteristics in the crystal growth, we have got the guideline to control the properties of solid solution semiconductors like ZnSe/CIGS thin films.

Acknowledgment

The authors would like to thank our supervisors, Prof. Koichi Yamashita and Prof. Kazunari Domen, for their agreements and great supports on this joint research. We are also grateful to MERIT program for giving us this invaluable research opportunity.

References

[1] Walter, M. G. *et al.* Solar water splitting cells. *Chem. Rev.* **110**, 6446–6473 (2010).

[2] Kaneko, H. *et al.* A novel photocathode

material for sunlight-driven overall water splitting: solid solution of ZnSe and Cu(In,Ga)Se_2. *Adv. Funct. Mater.* **26**, 4570–4577 (2016).

[3] Kaneko, H. *et al.* Enhanced hydrogen evolution under simulated sunlight from neutral electrolytes on $(ZnSe)_{0.85}(CuIn_{0.7}Ga_{0.3}Se_2)_{0.15}$ photocathodes prepared by a bilayer method. *Angew. Chemie Int. Ed.* **55**, 15329–15333 (2016).

[4] Zhao, Y. J. *et al.* Why can $CuInSe_2$ be readily equilibrium-doped n-type but the wider-gap $CuGaSe_2$ cannot? *Appl. Phys. Lett.* **85**, 5860 (2004).

[5] Kaneko, H. *et al.* Effects of Zn- and Cu-related defects in $(ZnSe)_x(CuIn_{0.7}Ga_{0.3}Se_2)_{1-x}$ thin film photocathodes on the photoelectrochemical properties for hydrogen production. *"Defects in semiconductors" Gordon Research Conference*, Colby-Sawyer College, New London, USA (2016)

[6] Andreev, A. *et al.* Synthesis and some properties of single crystals of $Zn_xCd_{1-x}S$ and ZnS_ySe_{1-y} solid solutions *Russ. J. Inorg. Chem.* 40, 1039-1042 (1995).

[7] Chen, S. *et al.* Electronic structure and stability of quaternary chalcogenide semiconductors derived from cation cross-substitution of II-VI and I-III-VI_2 compounds. *Phys. Rev. B* **79**, 165211 (2009).

[8] David R. Lide, ed., *CRC Handbook of Chemistry and Physics, Internet Version 2005*, <http://www.hbcpnetbase.com>, CRC Press, Boca Raton, FL, 2005.

[9] Turowski, M. *et al.* Photoemission studies of $CuInSe_2$ and $CuGaSe_2$ and of their interfaces with Si and Ge. *Phys. Rev. B* **31**, 1022 (1985).

[10] Ley, L. *et al.* Total valence-band densities of states of III-V and II-VI compounds from x-ray photoemission spectroscopy. *Phys. Rev. B* **9**, 600 (1974).